BioMedInformatics

MDPI

Article

Identifying Potent Fat Mass and Obesity-Associated Protein Inhibitors Using Deep Learning-Based Hybrid Procedures

Kannan Mayuri [1,2], Durairaj Varalakshmi [3], Mayakrishnan Tharaheswari [3], Chaitanya Sree Somala [2], Selvaraj Sathya Priya [2,4], Nagaraj Bharathkumar [2], Renganathan Senthil [5], Raja Babu Singh Kushwah [2], Sundaram Vickram [1,*], Thirunavukarasou Anand [2,4,*] and Konda Mani Saravanan [6,*]

1 Department of Biotechnology, Saveetha School of Engineering, Saveetha Institute of Medical and Technical Sciences (SIMATS), Thandalam, Chennai 602105, Tamil Nadu, India; pkmayurikannan@gmail.com
2 B Aatral Biosciences Private Limited, Bangalore 560091, Karnataka, India; schaitu27@gmail.com (C.S.S.); g.s.sathyapriya@gmail.com (S.S.P.); bharathkumarbcas@gmail.com (N.B.); rbskushwah001@gmail.com (R.B.S.K.)
3 Department of Biochemistry, Pondicherry University Community College, Pondicherry University, Pondicherry 605009, India; varuprofessor@gmail.com (D.V.); tharaniroopan7@gmail.com (M.T.)
4 SRIIC Lab, Central Research Facility, Sri Ramachandra Institute of Higher Education and Research, Chennai 600116, Tamil Nadu, India
5 Department of Bioinformatics, Vels Institute of Science Technology and Advanced Studies, Pallavaram, Chennai 600117, Tamil Nadu, India; rsenthil.sls@velsuniv.ac.in
6 Department of Biotechnology, Bharath Institute of Higher Education and Research, Chennai 600073, Tamil Nadu, India
* Correspondence: vickramas.sse@saveetha.com (S.V.); anand.t@baatral.com (T.A.); saravananbioinform@bharathuniv.ac.in (K.M.S.)

Abstract: The fat mass and obesity-associated (FTO) protein catalyzes metal-dependent modifications of nucleic acids, namely the demethylation of methyl adenosine inside mRNA molecules. The FTO protein has been identified as a potential target for developing anticancer therapies. Identifying a suitable ligand-targeting FTO protein is crucial to developing chemotherapeutic medicines to combat obesity and cancer. Scientists worldwide have employed many methodologies to discover a potent inhibitor for the FTO protein. This study uses deep learning-based methods and molecular docking techniques to investigate the FTO protein as a target. Our strategy involves systematically screening a database of small chemical compounds. By utilizing the crystal structures of the FTO complexed with ligands, we successfully identified three small-molecule chemical compounds (ZINC000003643476, ZINC000000517415, and ZINC000001562130) as inhibitors of the FTO protein. The identification process was accomplished by employing a combination of screening techniques, specifically deep learning (DeepBindGCN) and Autodock vina, on the ZINC database. These compounds were subjected to comprehensive analysis using 100 nanoseconds of molecular dynamics and binding free energy calculations. The findings of our study indicate the identification of three candidate inhibitors that might effectively target the human fat mass and obesity protein. The results of this study have the potential to facilitate the exploration of other chemicals that can interact with FTO. Conducting biochemical studies to evaluate these compounds' effectiveness may contribute to improving fat mass and obesity treatment strategies.

Keywords: FTO protein; deep learning-based screening; molecular docking; molecular simulations; drug screening

Key Contribution: By utilizing the crystal structures of the FTO complexed with ligands, we have successfully identified three small-molecule chemical compounds (ZINC000003643476, ZINC000000517415, and ZINC000001562130) as inhibitors of the FTO protein.

check for updates

Citation: Mayuri, K.; Varalakshmi, D.; Tharaheswari, M.; Somala, C.S.; Priya, S.S.; Bharathkumar, N.; Senthil, R.; Kushwah, R.B.S.; Vickram, S.; Anand, T.; et al. Identifying Potent Fat Mass and Obesity-Associated Protein Inhibitors Using Deep Learning-Based Hybrid Procedures. *BioMedInformatics* **2024**, *4*, 347–359. https://doi.org/10.3390/biomedinformatics4010020

Academic Editors: Alexandre G. De Brevern and Jörn Lötsch

Received: 2 November 2023
Revised: 20 December 2023
Accepted: 30 January 2024
Published: 1 February 2024

1. Introduction

The prevalence of obesity and cancer is steadily rising in numerous countries globally, posing a significant risk to human well-being [1,2]. Obesity induces alterations in the physiological and hormonal milieu of the body, thereby fostering the development of various diseases, such as diabetes and cardiovascular disorders [3]. Research has established a positive correlation between obesity and heightened susceptibility to a minimum of 13 distinct forms of cancer, including esophageal adenocarcinoma, colon cancer, endometrial cancer, postmenopausal breast cancer, kidney cancer, and hematopoietic cancers [4–11]. The molecular processes responsible for obesity and cancer involve obesity-related hormones, developmental factors, several signaling pathways, and chronic inflammation [12–14]. Fat mass and obesity-associated (FTO) gene cloning was initially accomplished through exon trapping analysis in mice with the fused-toes mutation [15–17]. The Genome-Wide Association Studies (GWAS) conducted in 2007 identified FTO as a gene influencing obesity susceptibility [18]. Specifically, several single-nucleotide polymorphisms (SNPs) located in the intron 1 region of the FTO gene were significantly associated with various anthropometric and dietary measures, including body mass index, body fat percentage, waist circumference, hip circumference, and energy intake. Consequently, the gene has been designated the FTO gene and has garnered significant scholarly interest [19,20].

Based on contemporary genomics research, it has been observed that the FTO gene is exclusively present in vertebrates and a limited number of marine algae species, exhibiting a remarkably conserved arrangement of nucleotides and amino acids [21–23]. The FTO gene, which is responsible for encoding a dioxygenase enzyme belonging to the AlkB family and dependent on 2-oxoglutarate (2-OG) Fe(II), is situated on chromosome 16q12.2 [24]. The FTO gene exhibits significant expression in adipose tissues and skeletal muscles within human anatomical structures [25]. Notably, the highest expression level is observed in the hypothalamus, specifically in the arcuate nucleus, which governs energy balance [26]. This finding suggests that FTO likely plays a crucial role in regulating appetite and energy metabolism [27]. Through the implementation of GWAS analysis, scholars have discovered a significant correlation between single-nucleotide polymorphisms (SNPs) in the FTO gene and the presence of obesity, as well as increased susceptibility to a range of cancers within populations of diverse racial backgrounds [28,29].

The FTO gene exhibits significant upregulation in various cancer tissues, functioning as an oncogene in an m6A-dependent manner and contributing to the modulation of cancer cells' malignant phenotype [30–33]. In a study conducted in 2017, Li and colleagues discovered that FTO, a protein-coding gene, played a role in promoting cell transformation and leukemogenesis induced by the leukemia oncogene [34,35]. The crystallographic analysis of human FTO complexed with a ligand elucidates a previously unidentified binding site for the FTO inhibitor. It provides insights into the molecular mechanisms underlying the recognition of the inhibitor by FTO [36,37]. The discovery of the novel binding site presents promising prospects for advancing targeted and potent FTO inhibitors [38]. This development will yield valuable insights into identifying potential therapeutic targets in discovering new drugs for obesity and related disorders [39].

In recent years, drug discovery research has seen extensive utilization of deep learning techniques [40,41]. Precisely and effectively predicting the interaction between proteins and ligands using computational methods is a fundamental aspect of extensive drug screening [42]. Given the advancements in deep learning algorithms and the growing availability of protein–ligand interaction data, particularly in high-resolution atomic structure and experimental binding affinity information, it is now feasible to utilize deep learning techniques to differentiate between binders and non-binders and predict the binding affinity [43]. In addition, we have developed DeepBindBC, which can determine whether protein–ligand complexes are native-like. This is accomplished by generating a comprehensive protein–ligand decoy complex as a negative training set [43,44]. The graph convolutional network (GCN) is a widely recognized deep learning technique that utilizes

nodes to store feature information and edges to represent spatial relationships between the nodes [45]. The application of the GCN in predicting chemical properties and molecular fingerprints has been extensively explored [46]. Moreover, the GCN has proven effective in predicting protein–ligand interactions [47]. In our recent work, we presented a screening process that combines DeepBindGCN with other techniques to identify molecules with a high affinity for binding, using TIPE3 and PD-L1 dimer as examples to demonstrate this approach [48]. One advantage of DeepBindGCN is its ability to operate without relying on specific docking conformations. Additionally, it effectively preserves both spatial information and physicochemical characteristics. In this study, we utilized the pocket residues or ligand atoms as the nodes and established edges based on the neighboring information to represent the protein pocket or ligand information comprehensively. Furthermore, the model utilizing pre-trained molecular vectors exhibited superior performance compared to the one-hot representation model. This method demonstrated better predictive ability than the most advanced affinity prediction models that depend on the three-dimensional complex. DeepBindGCN is a robust technique for predicting protein–ligand interactions and can be applied in several significant large-scale virtual screening scenarios. Researchers worldwide employ contemporary methodologies in conjunction with conventional ones to enhance the precision and efficacy of predictions [49,50].

Researchers have proposed a mixed approach for drug discovery called hybrid drug virtual screening [51]. For example, the deep learning architecture encompassing the end-to-end network structure exhibits exceptional speed and accuracy in recognizing patterns [52,53]. Disease classification studies commonly employ classical neural networks and popular new models, such as AlexNet, GoogleNet, VGGNet, ResNet, and DenseNet models, to improve performance [54,55]. These models are frequently utilized as foundations for research, aiming to enhance performance by integrating other techniques. The present work combines deep machine learning, molecular docking, and molecular dynamics simulation to identify potential therapeutic candidates from chemical databases. This computational analysis examines candidate compounds with the potential to inhibit the FTO protein. The prediction is improved in terms of accuracy and efficiency by combining three computing approaches: (i) virtual screening of the existing chemicals database, (ii) deep learning, and (iii) molecular dynamics and free-energy calculations. This study aims to discover small-molecule chemical compounds that exhibit inhibitory properties against FTO. The computational analysis of ligands complexed with human FTO demonstrates that the newly discovered small molecule shows a specific binding mode with FTO. The discovery of the small molecule presents potential avenues for advancing the development of FTO inhibitors that are more discerning and efficacious.

2. Materials and Methods

2.1. Target and Ligand Information

The protein under investigation in the current research is the FTO protein. The protein was subjected to crystallization in the presence of ligands, namely 3-METHYLTHYMIDINE, N-OXALYLGLYCINE, and FE (II) ION. The crystal structure obtained (Protein Data Bank Identifier—3LFM) was derived using X-ray diffraction with a resolution of 2.75 Å. The protein comprises a total of 495 amino acids [56]. The FTO protein consists of an amino-terminal domain with structural similarities to the AlkB family and a carboxy-terminal region with a unique fold [57,58]. In contrast to the structural characteristics seen in other members of the AlkB protein family, FTO has a distinctive additional loop that extends over one side of the conserved jelly-roll motif. This investigation used the ZINC database as a virtual screening library (source: https://zinc.docking.org/ accessed on 15 September 2023). The chemicals in the database are substances available for purchase in ready-to-dock, three-dimensional versions [59]. ZINC offers a vast collection of more than 750 million compounds. These compounds may be conveniently searched for analogs within a minute [60].

2.2. Virtual Screening Procedure

DeepBindGCN, a deep learning model based on Graph Convolution Networks (GCN), performs comprehensive screening on an extensive dataset [48]. The GCN is a well-recognized deep learning technique that utilizes nodes to store residue information and edges to represent spatial relationships among the nodes. The use of GCN in predicting chemical properties and molecular fingerprints has been extensively explored in previous studies [43,61–63]. In addition, the GCN has shown efficacy in protein–ligand interaction prediction. This particular type is renowned for its exceptional efficiency and precision while carrying out such jobs. DeepBindGCN_BC is a binary classifier designed to distinguish between binders and non-binders. On the other hand, DeepBindGCN_RG serves as a predictor for protein–ligand binding affinity. The enhanced accuracy of DeepBindBC may be attributed to incorporating both physical–chemical and spatial characteristics into the protein–ligand interactions. The importance of protein–ligand complexes was ranked by employing three distinct scoring procedures: DeepBindGCN_BC, DeepBindGCN_RG, and Autodock Vina score. The crystal structure was prepared for molecular docking using the Autodock Tools [64,65]. The protein molecule was introduced into the designated computational environment, where the missing side chains and loops were generated, and the hydrogen bonding pattern of the protein structure was refined. Water molecules with a size less than 3 Å were eliminated. The structure's energy was verified by applying depreciation to the optimized crystal structure. The OPLS 2005 force field was used in all protocols [66]. The information about ligand-binding residues present in the crystal structure was used to specify a grid. The Autodock tool was used for the ligand preparation process of these derivatives. The hydrogen bonds were introduced, and the bond length was determined using the OPLS 2005 algorithm [67]. Molecular docking was conducted using Autodock Vina, resulting in the acquisition of 10 poses for each ligand. These poses were then recorded in a suitable format to facilitate further analysis. The protein–ligand interactions were shown using the Discovery Studio visualizer V4.0.100.13345 [68].

2.3. Molecular Dynamics Simulations

Force-field-based molecular dynamics (MD) simulations were used to conduct supplementary screening for the protein–ligand complexes exhibiting the highest scores. The protein–ligand complexes were produced using the Autodock Vina docking method. Following this, the ligand was subjected to alteration using the pymol program to guarantee its positioning in the suitable protonation state [69]. The molecular dynamics (MD) simulations were performed using an AMBER-99SB force field implemented in the Gromacs program [70]. The ligand's architecture and partial charges were synthesized using ACPYPE [71]. A dodecahedron box was constructed, with the structural complex placed in its central location. The box was then populated with TIP3P water molecules by following the methodology outlined in reference [72]. A minimum separation distance of 1 nanometer was defined between the protein molecule and the boundary of the simulation box. The Gromacs software program included counter-ions to attain charge neutrality. A cutoff distance of 14 Å was used to determine non-bonded van der Waals interactions. The LINCS algorithm used hydrogen atoms to restrict covalent interactions [73]. Energy minimization was performed with a step size of 0.001 nanoseconds. Subsequently, a simulation lasting 100 picoseconds was conducted using an isothermal–isovolumetric ensemble (NVT). This was followed by a 10-nanosecond simulation using an isothermal–isobaric ensemble (NPT) to achieve equilibrium for the water system. A molecular dynamics simulation using a non-polarizable tight-binding model was performed, whereby a production run of 100 nanoseconds was executed. A time step of 2 femtoseconds was used for the simulation. The simulation used a Parrinello–Rahman barostat and a modified Berendsen thermostat, operating at a constant temperature of 300 K and a pressure of 1 atm. The trajectory's root-mean-square deviation (RMSD) was computed using the Gromacs software 2023.1 tools.

2.4. Binding Free Energy Calculation

The binding free energy of the top three FTO–ligand complex structures was calculated using the molecular mechanics/Poisson–Boltzmann surface area (MMPBSA) approach, which relies on molecular dynamics trajectories [74]. The calculation of MM-PBSA free energy was performed for the three highest-ranked complexes of FTO–ligand complexes. The binding free energy was calculated using the MM/PBSA technique, implemented in the g_mmpbsa program. The computation was conducted using the last 20 nanoseconds of the trajectory, whereby 20 frames were chosen from each nanosecond. A 40-nanosecond NPT molecular dynamics simulation acquired the trajectory used in this study. The calculation of the binding free energy was performed using the following equation:

$$\Delta G \text{ bind} = E\_complex(minimized) - E\_ligand(minimized) - E\_receptor(minimized)$$

3. Results

3.1. Virtual Screening Results

In this study, we used the crystal structure of the FTO protein and its associated ligand as a guide to implementing a hybrid screening approach. We aimed to find small-molecule chemical compounds from the ZINC database that could bind to the FTO protein. Three small molecules, namely ZINC000003643476, ZINC000000517415, and ZINC000001562130, were found with a DeepBindGCN_RG score of less than 7 (Table 1). Table 1 displays DeepBindGCN_BC, a binary classifier that distinguishes between binders and non-binders, as well as DeepBindGCN_RG, which is a process that predicts the affinity between proteins and ligands. The only difference was that one output was a binary value ranging from 0 to 1, indicating categorization, while the other was a continuous value representing affinity prediction. The conformation that was taken into consideration was the docked conformation, which had a binding energy of −9.0 or higher. Further analysis was conducted on the three docked complexes for more detailed information. The compound ZINC000003643476 exhibits 18 interactions with the amino acid residues present in the FTO protein, whereas ZINC000000517415 and ZINC000001562130 demonstrate 19 and 16 interactions, respectively, with the protein molecule seen in Figure 1. The ligand ZINC000000517415 exhibits a higher number of interactions in comparison to the other ligands. Five hydrophobic contacts were identified between ZINC000000517415 and ZINC000001562130, but only four hydrophobic interactions were observed between ZINC000000517415 and the receptor. The hydrophobic interactions play a crucial role in protein–ligand interactions [75]. The hydrophobic carbon composition of a ligand mainly determines whether the ligand can initially enter the active site [76]. The precise conformation of these hydrophobic carbons with the geometry of the active site also guarantees the absence of undesired protein–ligand interactions resembling the target [77].

Table 1. Predicted DeepBindGCN_BC, DeepBindGCN_RG, and binding energy of compounds from ZINC database with FTO protein.

S.No	Compound	DeepBindGCN_BC	DeepBindGCN_RG	Binding Energy (kJ/mol)
1	MolPort-001-741-269_ZINC000003643476	1	9.079	−10.0
2	MolPort-002-508-662_ZINC000000517415	1	9.025	−9.7
3	MolPort-002-476-943_ZINC000001562130	1	7.666	−9.0
4	MolPort-002-507-418_ZINC000142857948	1	6.040	−7.1
5	MolPort-002-801-687_ZINC000001022034	1	9.036	−7.1
6	MolPort-001-739-485_ZINC000229938091	1	9.052	−6.9
7	MolPort-005-945-631_ZINC000013485421	1	9.002	−6.8
8	MolPort-001-736-557_ZINC000005447704	1	9.334	−6.8
9	MolPort-001-741-121_ZINC000075906045	1	9.031	−6.8
10	MolPort-001-832-299_ZINC000004521756	1	9.045	−6.7

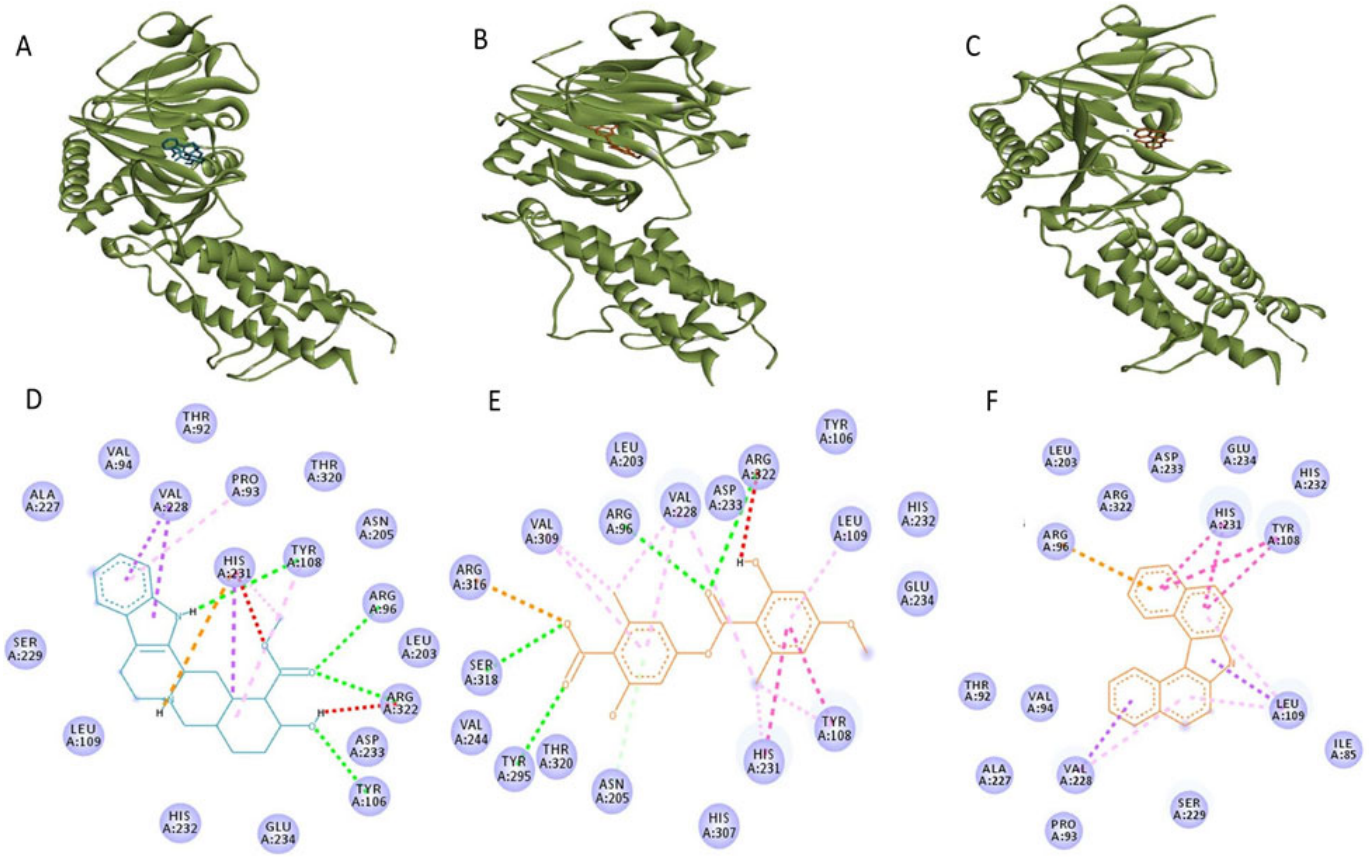

Figure 1. Schematic 3D (FTO-ZINC000003643476 (**A**), FTO-ZINC000000517415 (**B**), and FTO-ZINC000001562130 (**C**)) and 2D interaction diagrams of top three compounds with FTO protein (FTO-ZINC000003643476 (**D**), FTO-ZINC000000517415 (**E**), and FTO-ZINC000001562130 (**F**)).

Each of the three ligands exhibits an interaction with the leucine amino acid residue. The ligands establish interactions with leucine residues at positions 109 and 203 of the FTO protein. Charged residue interactions between the ligands and the receptor molecule involve arginine residues at positions 96 and 322 and an aspartic acid residue at position 233. Charged residues were discovered to enhance high-affinity binding. Additionally, they play a crucial role in "electrostatic steering", a technique that allows electrostatic forces to guide a ligand toward a binding site on the receptor protein, significantly increasing the association rate [78,79]. Our findings demonstrate the significance of the hydrophobic amino acid residue "Valine" at the 228th position. All three chemicals establish a strong hydrophobic interaction with the amino acid valine at position 228 and the charged residue arginine at position 96. Based on our empirical findings, it is evident that all the ligands exhibit a high degree of binding efficacy with the FTO protein, primarily due to their ability to establish a more significant number of stabilizing binding interactions.

Upon examination of the interactions between FTO and ligands in all three complexes, it is shown that a few interactions are conserved across all complexes. The amino acid residues 96Arg (positively charged) and 228Val, 203Leu, and 109Leu (hydrophobic) exhibit interactions with each of the three ligands, respectively. Shiraki and colleagues thoroughly address the involvement of the charged residue "Arginine" in protein–ligand interaction [80]. The interaction between a protein and a ligand via hydrophobic interactions is well recognized as a significant factor influencing the process of protein folding and stability. The significance of the histidine residue located at the interface is well acknowledged in preserving the appropriate conformation of the receptor for effective ligand binding.

3.2. Molecular Dynamics Simulations

Molecular Dynamics simulations were conducted on the three highest-ranked protein–ligand complexes acquired from molecular docking. Analyzed in Figure 2, the dynamic stability of the protein–ligand complex was estimated by examining the changes in root-mean-square deviation (RMSD) seen during the molecular dynamics (MD) simulations. The simulations accurately replicate the interactions and bonding within the protein–ligand complex while considering the environmental factors of water, temperature, and pressure in physiological settings. The protein–ligand complex was generated in the most favorable binding position obtained from docking, with an average root-mean-square deviation (RMSD) value of approximately 0.3 Å. A protein's backbone root-mean-square deviation (RMSD) falling between 0.2 and 0.4 Å is considered acceptable and provides vital information about the sequence of structural changes. The observed protein–ligand complex was found to be stable during the simulation time.

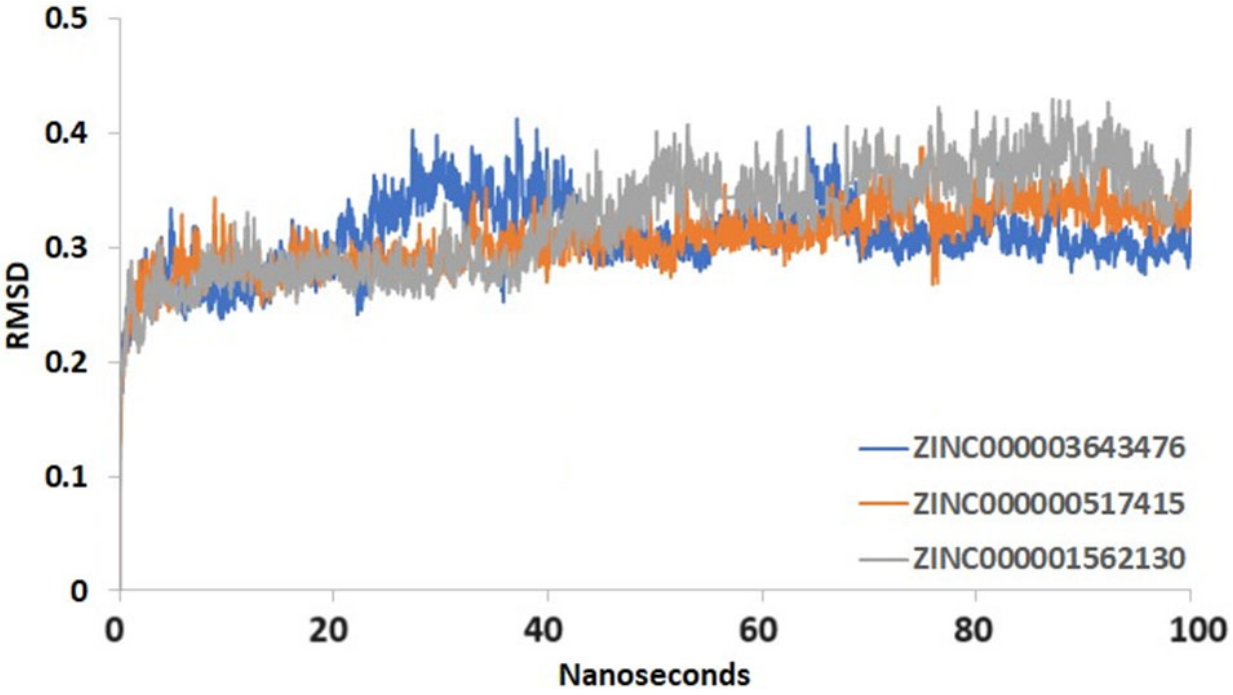

Figure 2. The root-mean-square deviation of the top three protein–ligand complexes for 100 ns atomic molecular dynamics simulations.

Figure 3 displays the root-mean-square fluctuation (RMSF) values for each amino acid residue in protein. The peaks shown in the figure represent the localized variations occurring throughout the protein chain. The observed RMSF values indicate that minor structural changes occurred inside the docking complex during the simulations. The interactions between the ligand atom and the protein residues throughout the simulation are seen in Figure 3. During the simulation, it was observed that the arginine residue at the 322nd position had interactions with ligand atoms for a duration exceeding 30% of the simulation time. Acknowledging that the residues above establish interactions during docking tests is essential. Additional mutagenesis investigations would provide a valuable opportunity to elucidate how ligands interact with critical binding amino acid residues.

3.3. Binding Free Energy

A highly effective method for verifying the accuracy of molecular docking outcomes involves the computation of the binding free energy of the protein–ligand complex using MM-PBSA continuum solvation. The MM-PBSA methodology was employed to determine the physical characteristics of three protein–ligand complexes. The molecular dynamics

(MD) trajectories were used to predict the binding energies (Figure 4). The diagram incorporates stabilizing physical free energy, including van der Waals forces, electrostatic interactions, and solvent-accessible surface area (SASA). ZINC000003643476 exhibited higher values of binding free energy (−104.14 kJ/mol), van der Waals (−193.42 kJ/mol) and electrostatic (−36.12 kJ/mol) free energies, and SASA (solvent-accessible surface area) free energy (−16.46 kJ/mol).

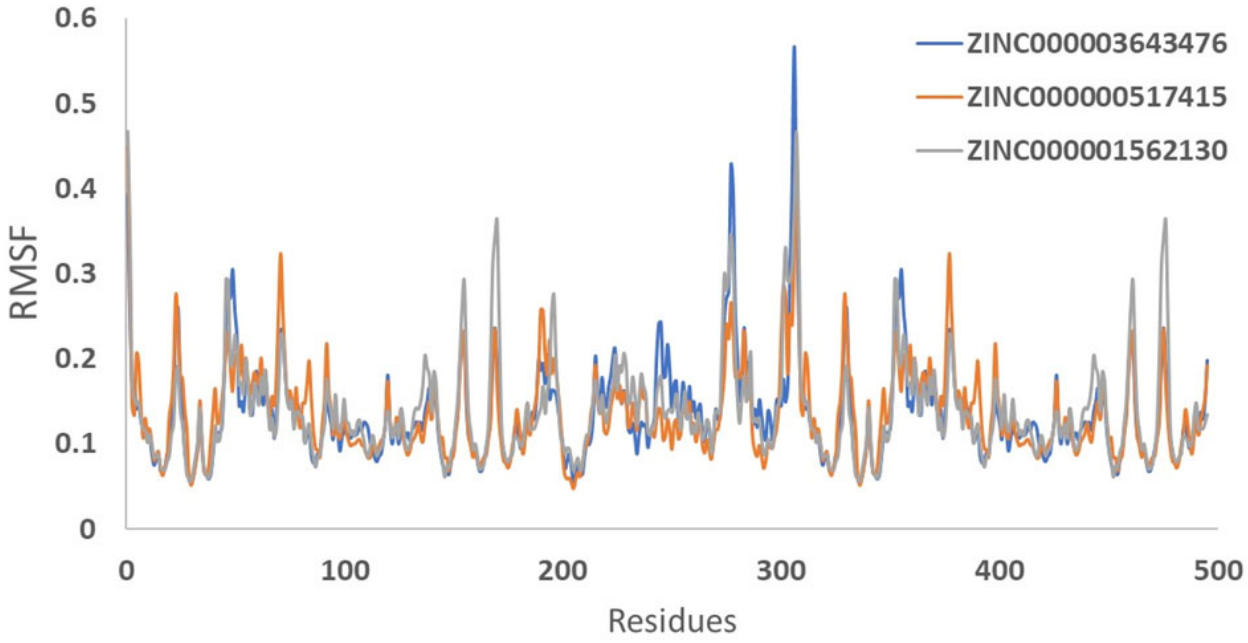

Figure 3. The root-mean-square fluctuation of the fat mass and obesity-associated protein.

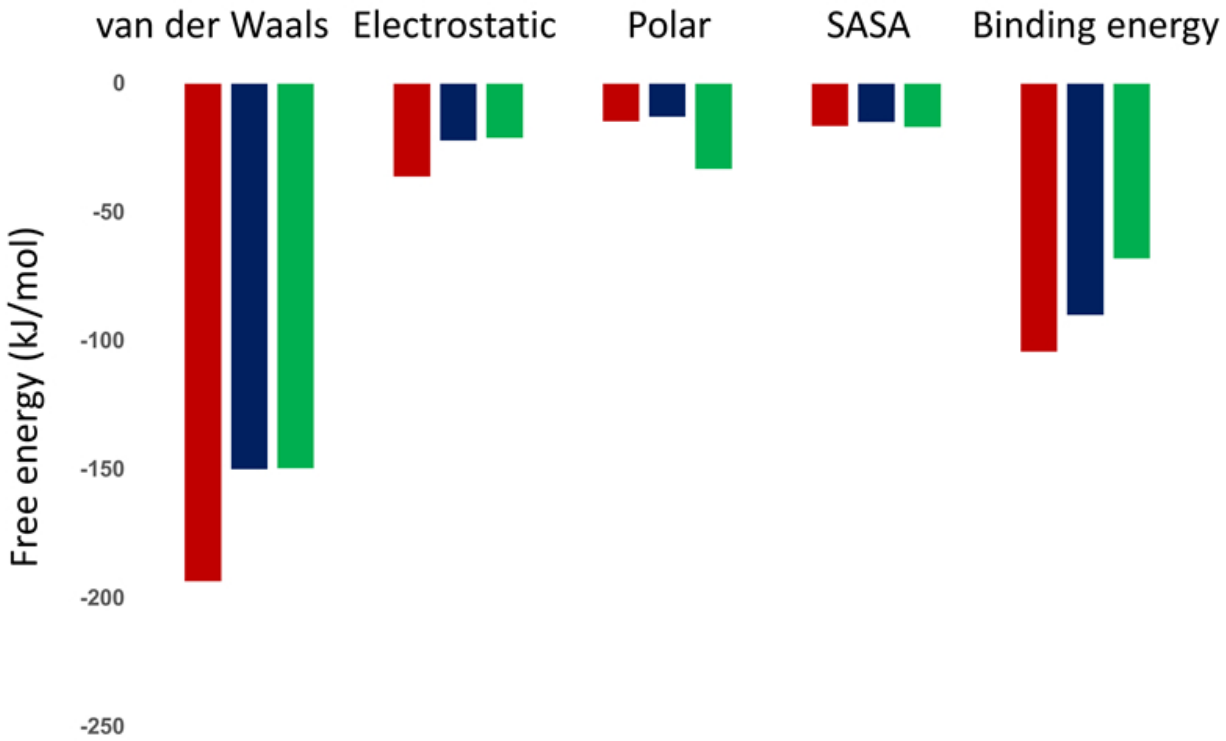

Figure 4. The calculated energy between protein and ligands was obtained by the MMPBSA method. The red color indicates the free energy of ZINC000003643476, the blue color indicates the free energy of ZINC000000517415, and the green color indicates the free energy of ZINC000001562130, respectively).

4. Discussion

Computer-aided drug screening can significantly enhance the process of identifying potential drug leads [81]. Discovering potent inhibitors with a restricted number of studies would pose a challenge [82]. According to the literature, molecular modeling and molecular dynamics simulations are highly effective in reducing the number of potential FTO inhibitors while still being computationally efficient [83]. Drug virtual screening has a lengthy and extensive history, encompassing the development of various related techniques like docking, Quantitative Structure Activity Relationship (QSAR), pharmacophore, and structure-based ligand similarity [84]. The increasing availability of deep learning algorithms and the growing collection of experimental protein–ligand interaction data will significantly enhance the use of deep learning for virtual drug screening [85]. Currently, protein-ligand interaction models utilize a graphical representation of ligands or proteins to capture their spatial and physical–chemical characteristics concisely [86]. These models employ a graph convolution network as the training architecture. The present study used a more efficient integrated virtual screening technique. Nevertheless, contemporary deep learning algorithms have already been utilized to identify inhibitors, and exhibit immense potential in drug development. Regardless, other constraints still require consideration, encompassing both efficiency and accuracy [48].

In addition, molecular dynamics simulations provide a higher level of atomic resolution for protein–ligand interaction, enhancing the predictability and facilitating the identification of ligand-binding processes. To summarize, we conducted screenings of small-molecule chemical databases to identify compounds with specific drug-like characteristics that can effectively block the FTO protein. The retrieved hits underwent several computational techniques, such as molecular dynamics simulations and free energy calculations. Our findings indicate three chemical compounds that can expedite medication development targeting the FTO protein. The results of our study can significantly assist in identifying potential compounds from a vast chemical pool, thereby facilitating the discovery of novel chemicals targeting the FTO protein.

Our group has recently published a series of research articles that focus on the recommendation of potential small-molecule chemical compounds for various target proteins [43,44,48,63,87]. This recommendation process is facilitated by our pipeline, which incorporates deep learning-based drug-screening techniques. The compounds that emerged as the best performers were selected for further study. Molecular dynamics (MD) simulations were used to investigate the protein–ligand complexes with the highest affinity to give more validation for the screening outcomes. The simulations were conducted for a duration of 100 nanoseconds. During the simulation, a modification was seen in the configuration of the docking complexes. Nevertheless, the ligands mostly remained confined to the FTO-binding area. Several van der Waals interactions facilitate the stabilization of FTO-ligand complexes. MD simulations determined the compounds' stability, wherein an in-depth analysis of protein–ligand complexes was conducted during the simulation period. The free energies obtained from the molecular mechanics/Poisson–Boltzmann surface area (MMPBSA) calculations provide further evidence to corroborate the findings of the screening process.

5. Conclusions

We utilize our advanced deep learning model, DeepBindGCN_BC, to precisely detect protein–ligand interaction. In addition, we employ DeepBindGCN_RG to evaluate the binding affinity between the FTO protein and ligands. Our GCN-based model enhances the identification of FTO inhibitors, especially those with strong binding affinity, which are often more favorable candidates for drug development. These models employ the graph convolution network to improve the effectiveness of spatial information representation. Further, molecular dynamics (MD) simulations and free energy calculations suggest that the compounds ZINC000003643476, ZINC000000517415, and ZINC000001562130 have significant potential as candidates for targeting the FTO protein in terms of binding and

stability. Furthermore, this study offers comprehensive insights into the interactions between proteins and ligands, which may greatly aid in drug development. The subsequent step in advancing this study is conducting experimental studies to validate the suggested potential compounds.

Author Contributions: Formal Analysis, N.B., R.S., T.A. and K.M.S.; Investigation, S.V.; Methodology, K.M., D.V. and M.T.; Software, K.M.S.; Supervision, S.V.; Validation, C.S.S., S.S.P. and T.A.; Writing—Original Draft, K.M.S.; Writing—Review and Editing, R.B.S.K., T.A. and K.M.S. All authors have read and agreed to the published version of the manuscript.

Funding: This research received no external funding.

Institutional Review Board Statement: Not applicable.

Informed Consent Statement: Not applicable.

Data Availability Statement: Data are contained within the article.

Conflicts of Interest: Authors Kannan Mayuri, Chaitanya Sree Somala, Selvaraj Sathya Priya, Nagaraj Bharathkumar, Raja Babu Singh Kushwah and Thirunavukarasou Anand were employed by the company B Aatral Biosciences Private Limited. The remaining authors declare that the research was conducted in the absence of any commercial or financial relationships that could be construed as a potential conflict of interest.

References

1. Ramachandran, A.; Snehalatha, C.; Satyavani, K.; Sivasankari, S.; Vijay, V. Type 2 Diabetes in Asian-Indian Urban Children. *Diabetes Care* **2003**, *26*, 1022–1025. [CrossRef] [PubMed]
2. Ahmed, B.; Konje, J.C. The Epidemiology of Obesity in Reproduction. *Best Pract. Res. Clin. Obstet. Gynaecol.* **2023**, *89*, 102342. [CrossRef] [PubMed]
3. Gross, D.C.; Cheever, C.R.; Batsis, J.A. Understanding the Development of Sarcopenic Obesity. *Expert Rev. Endocrinol. Metab.* **2023**, *18*, 469–488. [CrossRef] [PubMed]
4. De Pergola, G.; Silvestris, F. Obesity as a Major Risk Factor for Cancer. *J. Obes.* **2013**, *2013*, 291546. [CrossRef] [PubMed]
5. Otsuka, K.; Nishiyama, H.; Kuriki, D.; Kawada, N.; Ochiya, T. Connecting the Dots in the Associations between Diet, Obesity, Cancer, and MicroRNAs. *Semin. Cancer Biol.* **2023**, *93*, 52–69. [CrossRef] [PubMed]
6. Bupesh, G.; Saravanan, K.; Panneerselvam, G.; Meenakshi Sundaram, K.; Visvanathan, P. Role of Glucose Transporting Phytosterols in Diabetic Management. *Diabetes Obes. Int. J.* **2022**, *7*, 000261. [CrossRef]
7. Relier, S.; Rivals, E.; David, A. The Multifaceted Functions of the Fat Mass and Obesity-Associated Protein (FTO) in Normal and Cancer Cells. *RNA Biol.* **2022**, *19*, 132–142. [CrossRef]
8. Wei, H.; Li, Z.; Liu, F.; Wang, Y.; Ding, S.; Chen, Y.; Liu, J. The Role of FTO in Tumors and Its Research Progress. *Curr. Med. Chem.* **2022**, *29*, 924–933. [CrossRef]
9. Zuidhof, H.R.; Calkhoven, C.F. Oncogenic and Tumor-Suppressive Functions of the RNA Demethylase FTO. *Cancer Res.* **2022**, *82*, 2201–2212. [CrossRef]
10. Akbari, M.E.; Gholamalizadeh, M.; Doaei, S.; Mirsafa, F. FTO Gene Affects Obesity and Breast Cancer Through Similar Mechanisms: A New Insight into the Molecular Therapeutic Targets. *Nutr. Cancer* **2018**, *70*, 30–36. [CrossRef]
11. Chen, J.; Du, B. Novel Positioning from Obesity to Cancer: FTO, an M6A RNA Demethylase, Regulates Tumour Progression. *J. Cancer Res. Clin. Oncol.* **2019**, *145*, 19–29. [CrossRef] [PubMed]
12. Arvanitakis, K.; Papadakos, S.P.; Lekakis, V.; Koufakis, T.; Lempesis, I.G.; Papantoniou, E.; Kalopitas, G.; Georgakopoulou, V.E.; Stergiou, I.E.; Theocharis, S.; et al. Meeting at the Crossroad between Obesity and Hepatic Carcinogenesis: Unique Pathophysiological Pathways Raise Expectations for Innovative Therapeutic Approaches. *Int. J. Mol. Sci.* **2023**, *24*, 14704. [CrossRef] [PubMed]
13. Yang, Z.; Yu, G.; Zhu, X.; Peng, T.; Lv, Y. Critical Roles of FTO-Mediated MRNA M6A Demethylation in Regulating Adipogenesis and Lipid Metabolism: Implications in Lipid Metabolic Disorders. *Genes Dis.* **2022**, *9*, 51–61. [CrossRef]
14. Zhao, L.; Kong, X.; Zhong, W.; Wang, Y.; Li, P. FTO Accelerates Ovarian Cancer Cell Growth by Promoting Proliferation, Inhibiting Apoptosis, and Activating Autophagy. *Pathol.-Res. Pract.* **2020**, *216*, 153042. [CrossRef] [PubMed]
15. Huang, C.; Chen, W.; Wang, X. Studies on the Fat Mass and Obesity-Associated (FTO) Gene and Its Impact on Obesity-Associated Diseases. *Genes Dis.* **2023**, *10*, 2351–2365. [CrossRef]
16. Peters, T.; Ausmeier, K.; Rüther, U. Cloning of Fatso (Fto), a Novel Gene Deleted by the Fused Toes (Ft) Mouse Mutation. *Mamm. Genome* **1999**, *10*, 983–986. [CrossRef]
17. Deng, X.; Su, R.; Stanford, S.; Chen, J. Critical Enzymatic Functions of FTO in Obesity and Cancer. *Front. Endocrinol.* **2018**, *9*, 396. [CrossRef]

18. Scuteri, A.; Sanna, S.; Chen, W.-M.; Uda, M.; Albai, G.; Strait, J.; Najjar, S.; Nagaraja, R.; Orrú, M.; Usala, G.; et al. Genome-Wide Association Scan Shows Genetic Variants in the FTO Gene Are Associated with Obesity-Related Traits. *PLOS Genet.* **2007**, *3*, e115. [CrossRef]
19. Frayling, T.M.; Timpson, N.J.; Weedon, M.N.; Zeggini, E.; Freathy, R.M.; Lindgren, C.M.; Perry, J.R.B.; Elliott, K.S.; Lango, H.; Rayner, N.W.; et al. A Common Variant in the FTO Gene Is Associated with Body Mass Index and Predisposes to Childhood and Adult Obesity. *Science* **2007**, *316*, 889–894. [CrossRef]
20. Qiao, Y.; Zhou, B.; Zhang, M.; Liu, W.; Han, Z.; Song, C.; Yu, W.; Yang, Q.; Wang, R.; Wang, S.; et al. A Novel Inhibitor of the Obesity-Related Protein FTO. *Biochemistry* **2016**, *55*, 1516–1522. [CrossRef]
21. Ho, T.L.; Lee, J.; Ahn, S.Y.; Lee, D.-H.; Song, W.-J.; Kang, I.; Ko, E.-J. Immunostimulatory Effects of Marine Algae Extracts on in Vitro Antigen-presenting Cell Activation and in Vivo Immune Cell Recruitment. *Food Sci. Nutr.* **2023**, *11*, 6560–6570. [CrossRef]
22. Ruud, J.; Alber, J.; Tokarska, A.; Engström Ruud, L.; Nolte, H.; Biglari, N.; Lippert, R.; Lautenschlager, Ä.; Cieślak, P.E.; Szumiec, Ł.; et al. The Fat Mass and Obesity-Associated Protein (FTO) Regulates Locomotor Responses to Novelty via D2R Medium Spiny Neurons. *Cell Rep.* **2019**, *27*, 3182–3198.e9. [CrossRef]
23. Zhu, Y.; Zhou, G.; Yu, X.; Xu, Q.; Wang, K.; Xie, D.; Yang, Q.; Wang, L. LC-MS-MS Quantitative Analysis Reveals the Association between FTO and DNA Methylation. *PLoS ONE* **2017**, *12*, e0175849. [CrossRef]
24. Aik, W.; Scotti, J.S.; Choi, H.; Gong, L.; Demetriades, M.; Schofield, C.J.; McDonough, M.A. Structure of Human RNA N6-Methyladenine Demethylase ALKBH5 Provides Insights into Its Mechanisms of Nucleic Acid Recognition and Demethylation. *Nucleic Acids Res.* **2014**, *42*, 4741–4754. [CrossRef] [PubMed]
25. Ren, Y.; Li, Z.; Li, J.; Liang, R.; Wang, Z.; Bai, Y.; Yang, Y.; Tang, Q.; Fu, Y.; Zhang, X.; et al. M 6 A MRNA Methylation: Biological Features, Mechanisms, and Therapeutic Potentials in Type 2 Diabetes Mellitus. *Obes. Rev.* **2023**, *24*, e13639. [CrossRef] [PubMed]
26. Hu, F.; Yan, H.-J.; Gao, C.-X.; Sun, W.-W.; Long, Y.-S. Inhibition of Hypothalamic FTO Activates STAT3 Signal through ERK1/2 Associated with Reductions in Food Intake and Body Weight. *Neuroendocrinology* **2023**, *113*, 80–91. [CrossRef] [PubMed]
27. Sebert, S.; Salonurmi, T.; Keinänen-Kiukaanniemi, S.; Savolainen, M.; Herzig, K.-H.; Symonds, M.E.; Järvelin, M.-R. Programming Effects of FTO in the Development of Obesity. *Acta Physiol.* **2014**, *210*, 58–69. [CrossRef] [PubMed]
28. Farooq, S.; Rana, S.; Siddiqui, A.J.; Iqbal, A.; Bhatti, A.A.; Musharraf, S.G. Association of Lipid Metabolism-Related Metabolites with Overweight/Obesity Based on the FTO Rs1421085. *Mol. Omi.* **2023**, *19*, 697–705. [CrossRef] [PubMed]
29. Xie, G.; Wu, X.-N.; Ling, Y.; Rui, Y.; Wu, D.; Zhou, J.; Li, J.; Lin, S.; Peng, Q.; Li, Z.; et al. A Novel Inhibitor of N6-Methyladenosine Demethylase FTO Induces MRNA Methylation and Shows Anti-Cancer Activities. *Acta Pharm. Sin. B* **2022**, *12*, 853–866. [CrossRef]
30. Zheng, Q.-K.; Ma, C.; ullah, I.; Hu, K.; Ma, R.-J.; Zhang, N.; Sun, Z.-G. Roles of N6-Methyladenosine Demethylase FTO in Malignant Tumors Progression. *Onco. Targets. Ther.* **2021**, *14*, 4837–4846. [CrossRef] [PubMed]
31. Azzam, S.K.; Alsafar, H.; Sajini, A.A. FTO M6A Demethylase in Obesity and Cancer: Implications and Underlying Molecular Mechanisms. *Int. J. Mol. Sci.* **2022**, *23*, 3800. [CrossRef]
32. Ferenc, K.; Pilžys, T.; Garbicz, D.; Marcinkowski, M.; Skorobogatov, O.; Dylewska, M.; Gajewski, Z.; Grzesiuk, E.; Zabielski, R. Intracellular and Tissue Specific Expression of FTO Protein in Pig: Changes with Age, Energy Intake and Metabolic Status. *Sci. Rep.* **2020**, *10*, 13029. [CrossRef]
33. Lai, G.-Q.; Zhou, L.-L.; Yang, C.-G. RNA Methylation M6A: A New Code and Drug Target? *Chin. J. Chem.* **2020**, *38*, 420–421. [CrossRef]
34. Li, Z.; Weng, H.; Su, R.; Weng, X.; Zuo, Z.; Li, C.; Huang, H.; Nachtergaele, S.; Dong, L.; Hu, C.; et al. FTO Plays an Oncogenic Role in Acute Myeloid Leukemia as a N6-Methyladenosine RNA Demethylase. *Cancer Cell* **2017**, *31*, 127–141. [CrossRef]
35. Huang, Y.; Su, R.; Sheng, Y.; Dong, L.; Dong, Z.; Xu, H.; Ni, T.; Zhang, Z.S.; Zhang, T.; Li, C.; et al. Small-Molecule Targeting of Oncogenic FTO Demethylase in Acute Myeloid Leukemia. *Cancer Cell* **2019**, *35*, 677–691. [CrossRef]
36. He, W.; Zhou, B.; Liu, W.; Zhang, M.; Shen, Z.; Han, Z.; Jiang, Q.; Yang, Q.; Song, C.; Wang, R.; et al. Identification of A Novel Small-Molecule Binding Site of the Fat Mass and Obesity Associated Protein (FTO). *J. Med. Chem.* **2015**, *58*, 7341–7348. [CrossRef]
37. Gao, S.; Li, X.; Zhang, M.; Zhang, N.; Wang, R.; Chang, J. Structural Characteristics of Small-Molecule Inhibitors Targeting FTO Demethylase. *Future Med. Chem.* **2021**, *13*, 1475–1489. [CrossRef] [PubMed]
38. Shishodia, S.; Demetriades, M.; Zhang, D.; Tam, N.Y.; Maheswaran, P.; Clunie-O'Connor, C.; Tumber, A.; Leung, I.K.H.; Ng, Y.M.; Leissing, T.M.; et al. Structure-Based Design of Selective Fat Mass and Obesity Associated Protein (FTO) Inhibitors. *J. Med. Chem.* **2021**, *64*, 16609–16625. [CrossRef] [PubMed]
39. Huff, S.; Kummetha, I.R.; Zhang, L.; Wang, L.; Bray, W.; Yin, J.; Kelley, V.; Wang, Y.; Rana, T.M. Rational Design and Optimization of M6A-RNA Demethylase FTO Inhibitors as Anticancer Agents. *J. Med. Chem.* **2022**, *65*, 10920–10937. [CrossRef] [PubMed]
40. Askr, H.; Elgeldawi, E.; Aboul Ella, H.; Elshaier, Y.A.M.M.; Gomaa, M.M.; Hassanien, A.E. Deep Learning in Drug Discovery: An Integrative Review and Future Challenges. *Artif. Intell. Rev.* **2023**, *56*, 5975–6037. [CrossRef]
41. Zhang, H.; Saravanan, K.M.; Yang, Y.; Hossain, M.T.; Li, J.; Ren, X.; Pan, Y.; Wei, Y. Deep Learning Based Drug Screening for Novel Coronavirus 2019-NCov. *Interdiscip. Sci. Comput. Life Sci.* **2020**, *12*, 368–376. [CrossRef]
42. Zhang, H.; Li, J.; Saravanan, K.M.; Wu, H.; Wang, Z.; Wu, D.; Wei, Y.; Lu, Z.; Chen, Y.H.; Wan, X.; et al. An Integrated Deep Learning and Molecular Dynamics Simulation-Based Screening Pipeline Identifies Inhibitors of a New Cancer Drug Target TIPE2. *Front. Pharmacol.* **2021**, *12*, 772296. [CrossRef]

43. Zhang, H.; Zhang, T.; Saravanan, K.M.; Liao, L.; Wu, H.; Zhang, H.; Zhang, H.; Pan, Y.; Wu, X.; Wei, Y. DeepBindBC: A Practical Deep Learning Method for Identifying Native-like Protein-Ligand Complexes in Virtual Screening. *Methods* **2022**, *205*, 247–262. [CrossRef] [PubMed]
44. Zhang, H.; Saravanan, K.M.; Lin, J.; Liao, L.; Ng, J.T.-Y.; Zhou, J.; Wei, Y. DeepBindPoc: A Deep Learning Method to Rank Ligand Binding Pockets Using Molecular Vector Representation. *PeerJ* **2020**, *8*, e8864. [CrossRef] [PubMed]
45. Bhatti, U.A.; Tang, H.; Wu, G.; Marjan, S.; Hussain, A. Deep Learning with Graph Convolutional Networks: An Overview and Latest Applications in Computational Intelligence. *Int. J. Intell. Syst.* **2023**, *2023*, 8342104. [CrossRef]
46. Zhou, J.; Cui, G.; Hu, S.; Zhang, Z.; Yang, C.; Liu, Z.; Wang, L.; Li, C.; Sun, M. Graph Neural Networks: A Review of Methods and Applications. *AI Open* **2020**, *1*, 57–81. [CrossRef]
47. Puentes, P.R.; Rueda-Gensini, L.; Valderrama, N.; Hernández, I.; González, C.; Daza, L.; Muñoz-Camargo, C.; Cruz, J.C.; Arbeláez, P. Predicting Target–Ligand Interactions with Graph Convolutional Networks for Interpretable Pharmaceutical Discovery. *Sci. Rep.* **2022**, *12*, 8434. [CrossRef] [PubMed]
48. Zhang, H.; Saravanan, K.M.; Zhang, J.Z.H. DeepBindGCN: Integrating Molecular Vector Representation with Graph Convolutional Neural Networks for Protein–Ligand Interaction Prediction. *Molecules* **2023**, *28*, 4691. [CrossRef]
49. Dudek, G.; Pełka, P.; Smyl, S. A Hybrid Residual Dilated LSTM and Exponential Smoothing Model for Midterm Electric Load Forecasting. *IEEE Trans. Neural Netw. Learn. Syst.* **2022**, *33*, 2879–2891. [CrossRef]
50. Jalali, S.M.J.; Osório, G.J.; Ahmadian, S.; Lotfi, M.; Campos, V.M.A.; Shafie-khah, M.; Khosravi, A.; Catalão, J.P.S. New Hybrid Deep Neural Architectural Search-Based Ensemble Reinforcement Learning Strategy for Wind Power Forecasting. *IEEE Trans. Ind. Appl.* **2022**, *58*, 15–27. [CrossRef]
51. Feng, Y.; Cheng, X.; Wu, S.; Saravanan, K.M.; Liu, W. Hybrid Drug-Screening Strategy Identifies Potential SARS-CoV-2 Cell-Entry Inhibitors Targeting Human Transmembrane Serine Protease. *Struct. Chem.* **2022**, *33*, 1503–1515. [CrossRef]
52. Dai, G.; Tian, Z.; Fan, J.; Sunil, C.K.; Dewi, C. DFN-PSAN: Multi-Level Deep Information Feature Fusion Extraction Network for Interpretable Plant Disease Classification. *Comput. Electron. Agric.* **2024**, *216*, 108481. [CrossRef]
53. Chen, R.-C.; Dewi, C.; Zhuang, Y.-C.; Chen, J.-K. Contrast Limited Adaptive Histogram Equalization for Recognizing Road Marking at Night Based on Yolo Models. *IEEE Access* **2023**, *11*, 92926–92942. [CrossRef]
54. Fadafen, M.K.; Rezaee, K. Ensemble-Based Multi-Tissue Classification Approach of Colorectal Cancer Histology Images Using a Novel Hybrid Deep Learning Framework. *Sci. Rep.* **2023**, *13*, 8823. [CrossRef]
55. Dewi, C.; Chen, R.-C. Automatic Medical Face Mask Detection Based on Cross-Stage Partial Network to Combat COVID-19. *Big Data Cogn. Comput.* **2022**, *6*, 106. [CrossRef]
56. Berman, H.M.; Westbrook, J.; Feng, Z.; Gilliland, G.; Bhat, T.N.; Weissig, H.; Shindyalov, I.N.; Bourne, P.E. The Protein Data Bank. *Nucleic Acids Res.* **2000**, *28*, 235–242. [CrossRef] [PubMed]
57. Han, Z.; Niu, T.; Chang, J.; Lei, X.; Zhao, M.; Wang, Q.; Cheng, W.; Wang, J.; Feng, Y.; Chai, J. Crystal Structure of the FTO Protein Reveals Basis for Its Substrate Specificity. *Nature* **2010**, *464*, 1205–1209. [CrossRef] [PubMed]
58. Huang, Y.; Yan, J.; Li, Q.; Li, J.; Gong, S.; Zhou, H.; Gan, J.; Jiang, H.; Jia, G.-F.; Luo, C.; et al. Meclofenamic Acid Selectively Inhibits FTO Demethylation of M6A over ALKBH5. *Nucleic Acids Res.* **2015**, *43*, 373–384. [CrossRef] [PubMed]
59. Irwin, J.J.; Shoichet, B.K. ZINC—A Free Database of Commercially Available Compounds for Virtual Screening. *J. Chem. Inf. Model.* **2005**, *45*, 177–182. [CrossRef] [PubMed]
60. Irwin, J.J.; Sterling, T.; Mysinger, M.M.; Bolstad, E.S.; Coleman, R.G. ZINC: A Free Tool to Discover Chemistry for Biology. *J. Chem. Inf. Model.* **2012**, *52*, 1757–1768. [CrossRef] [PubMed]
61. Sun, M.; Zhao, S.; Gilvary, C.; Elemento, O.; Zhou, J.; Wang, F. Graph Convolutional Networks for Computational Drug Development and Discovery. *Brief. Bioinform.* **2020**, *21*, 919–935. [CrossRef]
62. Son, J.; Kim, D. Development of a Graph Convolutional Neural Network Model for Efficient Prediction of Protein-Ligand Binding Affinities. *PLoS ONE* **2021**, *16*, e0249404. [CrossRef]
63. Zhang, H.; Liao, L.; Saravanan, K.M.; Yin, P.; Wei, Y. DeepBindRG: A Deep Learning Based Method for Estimating Effective Protein–Ligand Affinity. *PeerJ* **2019**, *7*, e7362. [CrossRef]
64. Brooks, B.R., III; Mackerell, J.; Nilsson, L.; Petrella, R.J.; Roux, B.; Won, Y.; Archontis, G.; Bartels, C.; Boresch, S.; Caflisch, A.; et al. Autodock Vina. *J. Comput. Chem.* **2009**, *30*, 1545. [CrossRef]
65. Goodsell, D.S.; Sanner, M.F.; Olson, A.J.; Forli, S. The AutoDock Suite at 30. *Protein Sci.* **2021**, *30*, 31–43. [CrossRef]
66. Kaminski, G.; Jorgensen, W.L. Performance of the AMBER94, MMFF94, and OPLS-AA Force Fields for Modeling Organic Liquids. *J. Phys. Chem.* **1996**, *100*, 18010–18013. [CrossRef]
67. Harder, E.; Damm, W.; Maple, J.; Wu, C.; Reboul, M.; Xiang, J.Y.; Wang, L.; Lupyan, D.; Dahlgren, M.K.; Knight, J.L.; et al. OPLS3: A Force Field Providing Broad Coverage of Drug-like Small Molecules and Proteins. *J. Chem. Theory Comput.* **2016**, *12*, 281–296. [CrossRef] [PubMed]
68. *Discovery Studio Visualizer*, V4.0.100.13345; Accelrys Softw. Inc.: San Diego, CA, USA, 2005.
69. Lill, M.A.; Danielson, M.L. Computer-Aided Drug Design Platform Using PyMOL. *J. Comput. Aided. Mol. Des.* **2011**, *25*, 13–19. [CrossRef] [PubMed]
70. Hess, B.; Kutzner, C.; van der Spoel, D.; Lindahl, E. GROMACS 4: Algorithms for Highly Efficient, Load-Balanced, and Scalable Molecular Simulation. *J. Chem. Theory Comput.* **2008**, *4*, 435–447. [CrossRef] [PubMed]

71. da Silva, A.W.S.; Vranken, W.F. ACPYPE—AnteChamber PYthon Parser InterfacE. *BMC Res. Notes* **2012**, *5*, 367. [CrossRef] [PubMed]
72. Jorgensen, W.L.; Chandrasekhar, J.; Madura, J.D.; Impey, R.W.; Klein, M.L. Comparison of Simple Potential Functions for Simulating Liquid Water. *J. Chem. Phys.* **1983**, *79*, 926–935. [CrossRef]
73. Hess, B.; Bekker, H.; Berendsen, H.J.C.; Fraaije, J.G.E.M. LINCS: A Linear Constraint Solver for Molecular Simulations. *J. Comput. Chem.* **1997**, *18*, 1463–1472. [CrossRef]
74. Homeyer, N.; Gohlke, H. Free Energy Calculations by the Molecular Mechanics Poisson−Boltzmann Surface Area Method. *Mol. Inform.* **2012**, *31*, 114–122. [CrossRef]
75. Ferreira de Freitas, R.; Schapira, M. A Systematic Analysis of Atomic Protein–Ligand Interactions in the PDB. *Medchemcomm* **2017**, *8*, 1970–1981. [CrossRef]
76. Zhao, Z.; Bourne, P.E. Harnessing Systematic Protein–Ligand Interaction Fingerprints for Drug Discovery. *Drug Discov. Today* **2022**, *27*, 103319. [CrossRef]
77. Kuhlman, B.; Bradley, P. Advances in Protein Structure Prediction and Design. *Nat. Rev. Mol. Cell Biol.* **2019**, *20*, 681–697. [CrossRef] [PubMed]
78. Skolnick, J.; Zhou, H. Implications of the Essential Role of Small Molecule Ligand Binding Pockets in Protein–Protein Interactions. *J. Phys. Chem. B* **2022**, *126*, 6853–6867. [CrossRef] [PubMed]
79. Zhao, N.; Pang, B.; Shyu, C.-R.; Korkin, D. Charged Residues at Protein Interaction Interfaces: Unexpected Conservation and Orchestrated Divergence. *Protein Sci.* **2011**, *20*, 1275–1284. [CrossRef] [PubMed]
80. Hirano, A.; Kameda, T.; Arakawa, T.; Shiraki, K. Arginine-Assisted Solubilization System for Drug Substances: Solubility Experiment and Simulation. *J. Phys. Chem. B* **2010**, *114*, 13455–13462. [CrossRef]
81. Shiammala, P.N.; Duraimutharasan, N.K.B.; Vaseeharan, B.; Alothaim, A.S.; Al-Malki, E.S.; Snekaa, B.; Safi, S.Z.; Singh, S.K.; Velmurugan, D.; Selvaraj, C. Exploring the Artificial Intelligence and Machine Learning Models in the Context of Drug Design Difficulties and Future Potential for the Pharmaceutical Sectors. *Methods* **2023**, *219*, 82–94. [CrossRef] [PubMed]
82. Murugesan, A.; Mani, S.K.; Thiyagarajan, R.; Palanivel, S.; Gurbanov, A.V.; Zubkov, F.I.; Kandhavelu, M. Benzenesulfonamide Analogs: Synthesis, Anti-GBM Activity and Pharmacoprofiling. *Int. J. Mol. Sci.* **2023**, *24*, 12276. [CrossRef]
83. Kumar, S.U.; Rajan, B.; Kumar, D.T.; Cathryn, R.H.; Das, V.S.; Zayed, H.; Walter, C.E.J.; Ramanathan, G.; Doss, C.P.G. Comparison of Potential Inhibitors and Targeting Fat Mass and Obesity-Associated Protein Causing Diabesity through Docking and Molecular Dynamics Strategies. *J. Cell. Biochem.* **2021**, *122*, 1625–1638. [CrossRef] [PubMed]
84. Wang, Z.; Yang, B. *Strategies of Polypharmacology BT—Polypharmacology: Principles and Methodologies*; Wang, Z., Yang, B., Eds.; Springer International Publishing: Cham, Switzerland, 2022; pp. 43–72. ISBN 978-3-031-04998-9.
85. Isert, C.; Atz, K.; Schneider, G. Structure-Based Drug Design with Geometric Deep Learning. *Curr. Opin. Struct. Biol.* **2023**, *79*, 102548. [CrossRef] [PubMed]
86. Nguyen, T.; Le, H.; Quinn, T.P.; Nguyen, T.; Le, T.D.; Venkatesh, S. GraphDTA: Predicting Drug Target Binding Affinity with Graph Neural Networks. *Bioinformatics* **2021**, *37*, 1140–1147. [CrossRef] [PubMed]
87. Sreeraman, S.; Kannan, P.M.; Singh Kushwah, R.B.; Sundaram, V.; Veluchamy, A.; Thirunavukarasou, A.; Saravanan, M.K. Drug Design and Disease Diagnosis: The Potential of Deep Learning Models in Biology. *Curr. Bioinform.* **2023**, *18*, 208–220. [CrossRef]